Maximally localized Wannier functions constructed from projector-augmented waves or ultrasoft pseudopotentials

2007 J. Phys.: Condens. Matter 19 036215

(http://iopscience.iop.org/0953-8984/19/3/036215)

INSTITUTE OF PHYSICS PUBLISHING JOURNAL OF PHYSICS: CONDENSED MATTER

J. Phys.: Condens. Matter **19** (2007) 036215 (16pp) doi:10.1088/0953-8984/19/3/036215

Maximally localized Wannier functions constructed from projector-augmented waves or ultrasoft pseudopotentials

A Ferretti, A Calzolari, B Bonferroni and R Di Felice

National Centre on nanoStructures and bioSystems at Surfaces (S^3) of INFM-CNR, Dipartimento di Fisica, Università di Modena e Reggio Emilia, 41100 Modena, Italy

E-mail: ferretti.andrea@unimore.it

Received 7 August 2006, in final form 29 October 2006
Published 5 January 2007
Online at stacks.iop.org/JPhysCM/19/036215

Abstract

We report a theoretical scheme that enables the calculation of maximally localized Wannier functions within the formalism of projector-augmented waves (PAW), which also includes the ultrasoft pseudopotential (USPP) approach. We give a description of the basic underlying formalism and explicitly write out all the required matrix elements using the common ingredients of the PAW/USPP theory. We report an implementation of the method in a form suitable for accepting the input electronic structure from USPP plane-wave DFT simulations. We apply the method to the calculation of Wannier functions, dipole moments and spontaneous polarizations for a range of test cases. A comparison with norm-conserving pseudopotentials is reported as a benchmark.

(Some figures in this article are in colour only in the electronic version)

1. Introduction

Wannier functions (WFs) can be obtained by a unitary transformation of the extended wavefunctions of a periodic system [1, 2]. So far, the effective circulation/application of WFs in electronic structure calculations has been hindered by their intrinsic non-uniqueness [1, 2]. The related degrees of freedom can be chosen, e.g., by making use of the symmetry properties of the system, as proposed by [3] and lately by [4, 5]. In 1997 Marzari and Vanderbilt proposed a further approach [6, 7] for exploiting the non-uniqueness: the proposed methodology allows one to extract, from a selected manifold of bands, the set of WFs with the maximum spatial localization, i.e. the *maximally localized Wannier functions* (MLWFs). On one hand, MLWFs are attractive because they constitute a complete and orthonormal basis set with real space localization. On the other hand, with respect to other numerical real space bases, they also carry the physical information of the starting Bloch functions. Indeed, MLWFs may yield a

chemical view of molecular bond orbitals, and they can be exploited for the computation of the spontaneous polarization in periodic systems [8–10], becoming very popular for tackling these issues in advanced materials [11–13]. In addition, MLWFs have most recently been proposed for calculating the transport properties of nanosize conductors connected to external electrodes [14–18].

The calculation of MLWFs was originally implemented [6] for a projection from Bloch orbitals expanded on a plane-wave basis set in density functional theory (DFT) calculations, within the norm-conserving pseudopotential (NCPP) framework. Norm-conserving pseudopotentials [19, 20], that allow one to neglect core electrons in the evaluation of physical observables, are usually characterized by a high transferability of an element to a variety of chemical environments. However, the norm conservation in the core region is a strong constraint, that affects the computational effort of the DFT calculations. As a consequence, some chemical species, such as first-row elements (e.g. C, N, O, F) and especially transition metals (e.g. Mn, Fe, Co, Ni, Cu) and rare earths (e.g. La, Gd, Yb), require an extremely high number of basis functions (e.g. plane waves), in order to be described with a satisfactory accuracy. Unfortunately, the typical systems of interest in nanoscience and specifically in molecular electronics contain atoms of those critical species.

A first attempt to solve this problem within the pseudopotential framework was the use of ultrasoft pseudopotentials (USPPs) [21]. The norm conservation constraint is relaxed, allowing for a drastic reduction of the plane-wave kinetic energy cut-off. The price of this reduction is an increase of the complexity of the formalism; further *augmentation* terms [21] must be added for the computation of relevant matrix elements, in order to correct the *wrong* normalization of the wavefunctions. In parallel, the theory of projector-augmented waves (PAW) [22] offers an alternative more general framework including both pseudopotentials and augmented bases (like e.g. LAPW). Indeed, it has been demonstrated [22–24] that the USPP procedure may be mapped into the PAW theory and we refer the reader to the original papers for further details. We therefore extended the original Marzari–Vanderbilt [6] approach for MLWFs to the PAW scheme. This allows us on one hand to extend this technique to a larger electronic structure community, and on the other hand to compute MLWFs from USPP Bloch functions as a direct application of the general theory.

The paper is organized as follows: in section 2 we first write down the salient quantities that enter the computation of the WFs, and then we show the formal equivalence between PAW and USPP theories and express the MLWFs within such theories in a general framework; in section 3 we report the results of the application of our method to several test cases, that explore both the chemical bonding and the electrical polarization in the pertinent cases; finally we draw our conclusions in section 4.

2. Formalism

2.1. Maximally localized Wannier functions

In this section we give a brief introduction to the theory of maximally localized Wannier functions. A more detailed description can be found in the original papers [6, 7]. In the case of an isolated band, Wannier functions can be defined [1, 2] as a combination of the Bloch orbitals $|\psi_{\mathbf{k}}\rangle$ corresponding to different $\mathbf{k}$-points as follows:

$$|w_{\mathbf{R}}\rangle = \frac{V}{(2\pi)^3}\int_{\mathrm{BZ}} \mathrm{d}\mathbf{k}\, \mathrm{e}^{-\mathrm{i}\mathbf{k}\cdot\mathbf{R}}\mathrm{e}^{\mathrm{i}\phi_{\mathbf{k}}}|\psi_{\mathbf{k}}\rangle \tag{1}$$

where $e^{i\phi_{\mathbf{k}}}$ is a $\mathbf{k}$-dependent phase factor. This definition has been generalized [6] to a group of bands leading to the expression

$$|w_{\mathbf{R},m}\rangle = \frac{V}{(2\pi)^3}\int_{\mathrm{BZ}} d\mathbf{k} e^{-i\mathbf{k}\cdot\mathbf{R}} \sum_n U^{\mathbf{k}}_{nm}|\psi_{\mathbf{k},n}\rangle. \tag{2}$$

Here the extra degrees of freedom related to the phases of the Bloch eigenstates are collected in the unitary matrices $U^{\mathbf{k}}$. In the one-band case it has been demonstrated that a suitable choice of the phases $e^{i\phi_{\mathbf{k}}}$ leads to WFs which are real and exponentially decaying in a real space representation [2]. In the many-band case [25] this theorem does not hold any longer but the arbitrariness in the unitary (gauge) transformation $U^{\mathbf{k}}$ can be exploited. Following Marzari and Vanderbilt [6] we define a *spread* functional Ω, which gives a measure of the degree of localization of the WF set. It reads

$$\Omega\left[\{U^{\mathbf{k}}\}\right] = \sum_n \left[\langle \hat{r}^2\rangle_n - \langle \hat{\mathbf{r}}\rangle_n^2\right], \tag{3}$$

where $\langle\cdot\rangle_n$ is the expectation value of a given operator on the nth WF calculated using the $U^{\mathbf{k}}$ gauge transformation. It is therefore possible to define the *maximally localized* Wannier functions (MLWFs) as the WFs resulting from (2) by means of the unitary transformation $\{U^{\mathbf{k}}\}$ that minimizes the spread functional. The $\{U^{\mathbf{k}}\}$ matrices can be computed by the direct application of standard minimization algorithms (e.g. steepest-descent or conjugate-gradient approaches) on the functional $\Omega\left[\{U^{\mathbf{k}}\}\right]$. The related details have been fully discussed elsewhere [6].

According to the formal analysis of the $\langle\hat{\mathbf{r}}\rangle_n$ and $\langle\hat{r}^2\rangle_n$ terms given by Blount [26, 6], it is possible to demonstrate that the dependence of Ω on the gauge transformation is determined only by the so-called overlap integrals $M^{\mathbf{k},\mathbf{b}}$:

$$\begin{aligned} M^{\mathbf{k},\mathbf{b}}_{mn} &= \langle\psi_{\mathbf{k},m}|\, e^{-i\mathbf{b}\cdot\hat{\mathbf{r}}}\,|\psi_{\mathbf{k}+\mathbf{b},n}\rangle \\ &= \int_{\mathrm{Crystal}} d\mathbf{r}\, u^*_{\mathbf{k},m}(\mathbf{r}) u_{\mathbf{k}+\mathbf{b},n}(\mathbf{r}), \end{aligned} \tag{4}$$

$u_{\mathbf{k},m}(\mathbf{r})$ being the periodic part of the Bloch states $\psi_{\mathbf{k},m}(\mathbf{r}) = e^{i\mathbf{k}\cdot\mathbf{r}}\, u_{\mathbf{k},m}(\mathbf{r})$. Here we deal with a regularly discretized mesh of $\mathbf{k}$-points, where the $\mathbf{b}$-vectors connect nearest-neighbour $\mathbf{k}$-points. The detailed form of the position expectation values and of the spread functional (including its gradient w.r.t. to $U^{\mathbf{k}}$) in terms of the overlap integrals is reported in appendix A. Since the representation of Bloch eigenstates enters only the calculation of the $M^{\mathbf{k},\mathbf{b}}$ integrals, these quantities are the main objects to deal with when using a USPP or PAW formalism. The detailed treatment is reported in section 2.3.

2.2. *PAW and ultrasoft pseudopotentials*

The PAW formalism has been introduced by Blöchl [27, 28, 22] and it has also been demonstrated [24] that the Vanderbilt ultrasoft pseudopotential (USPP) theory [21, 29, 30, 23, 31] can be obtained within the PAW approach with some further approximations.

Blöchl's starting point is to partition the volume of the system by setting spherical regions (atomic spheres) around each atom. In each sphere two complete sets of wavelets[1] ($\{|\phi_i^{\mathrm{ae}}\rangle\}$ and $\{|\phi_i^{\mathrm{ps}}\rangle\}$) localized in the sphere are defined. While the former, when truncated, is intended to work with all-electron (AE) functions, the latter should be smoother and easily representable in plane waves. It is therefore possible to introduce a well defined linear operator mapping one-to-one AE-like functions into smoother pseudo-functions and vice versa:

[1] Wavelets have defined angular momentum (e.g. their angular parts are spherical harmonics), but are not supposed to be atomic eigenstates or even to be orthogonal.

$$|\psi^{\rm ae}\rangle = \hat{T}|\psi^{\rm ps}\rangle, \tag{5}$$

where

$$\hat{T} = \mathbb{I} + \sum_{I,i} \left(|\phi^{\rm ae}_{Ii}\rangle - |\phi^{\rm ps}_{Ii}\rangle\right) \langle\beta_{Ii}|. \tag{6}$$

The index I runs over different atoms (e.g. different atomic spheres), while $\langle\beta_{Ii}|$ are the projectors[2] related to the pseudo-wavelets $|\phi^{\rm ps}_{Ii}\rangle$. The $\hat{T}$ operator acts on the pseudized functions to reconstruct [23] the AE ones.

Matrix elements and expectation values of a generic operator $\hat{A}$ on the physical AE states can be written as

$$A_{mn} = \langle\psi^{\rm ps}_m|\hat{A}^{\rm ps}|\psi^{\rm ps}_n\rangle = \langle\psi^{\rm ps}_m|\hat{T}^\dagger\hat{A}\hat{T}|\psi^{\rm ps}_n\rangle. \tag{7}$$

One of the main results of [22] is the explicit expression for $\hat{A}^{\rm ps}$, which we report here for the case of local and semilocal operators:

$$\begin{aligned} \hat{A}^{\rm ps} &= \hat{A} + \hat{A}^{\rm aug}, \\ \hat{A}^{\rm aug} &= \sum_{I,ij} \left[\langle\phi^{\rm ae}_{Ii}|\hat{A}|\phi^{\rm ae}_{Ij}\rangle - \langle\phi^{\rm ps}_{Ii}|\hat{A}|\phi^{\rm ps}_{Ij}\rangle\right] |\beta_{Ii}\rangle\langle\beta_{Ij}|. \end{aligned} \tag{8}$$

The second term ($\hat{A}^{\rm aug}$) in the rhs of (8) takes into account the corrections due to the use of the pseudo-functions instead of the AE ones, and from here on it will be called the augmentation term. At this point it is useful to define the quantities $Q^I_{ij}(\mathbf{r})$ and q^I_{ij} (augmentation densities and charges respectively) as

$$Q^I_{ij}(\mathbf{r}) = \phi^{\rm ae*}_{Ii}(\mathbf{r})\,\phi^{\rm ae}_{Ij}(\mathbf{r}) - \phi^{\rm ps*}_{Ii}(\mathbf{r})\phi^{\rm ps}_{Ij}(\mathbf{r}), \tag{9}$$

$$q^I_{ij} = \int {\rm d}\mathbf{r}\, Q^I_{ij}(\mathbf{r}). \tag{10}$$

Within these definitions, (8) for local operators $A(\mathbf{r})$ can be recast in a more convenient form:

$$\hat{A}^{\rm aug} = \sum_{I,ij} \left[\int {\rm d}\mathbf{r}\, Q^I_{ij}(\mathbf{r}) A(\mathbf{r})\right] |\beta_{Ii}\rangle\langle\beta_{Ij}|. \tag{11}$$

Setting $\hat{A}$ to the identity in (8) and (11), scalar products are given by $\langle\psi^{\rm ps}_m|\hat{S}|\psi^{\rm ps}_n\rangle$ where the number operator[3] $\hat{S}$ (that characterizes also the USPP formalism) is given by

$$\hat{S} = \hat{T}^\dagger\hat{T} = \mathbb{I} + \sum_{I,ij} |\beta_{Ii}\rangle q^I_{ij} \langle\beta_{Ij}|. \tag{12}$$

In the same way, by setting $A(\mathbf{r}') = e\delta(\mathbf{r}' - \mathbf{r})$ we obtain an expression for the density:

$$\begin{aligned} n(\mathbf{r}) &= n^{\rm ps}(\mathbf{r}) + n^{\rm aug}(\mathbf{r}), \\ n^{\rm aug}(\mathbf{r}) &= \frac{2e}{N_{\mathbf{k}}} \sum_{m\mathbf{k}} \sum_{I,ij} \langle\psi^{\rm ps}_{\mathbf{k},m}|\beta_{Ii}\rangle Q^I_{ij}(\mathbf{r}) \langle\beta_{Ij}|\psi^{\rm ps}_{\mathbf{k},m}\rangle, \end{aligned} \tag{13}$$

where $n^{\rm ps}(\mathbf{r})$ is the density contribution of the pseudo-wavefunctions. Since we are able to express all the quantities of interest in terms of the soft pseudo-states, the quantum problem can be solved directly in this representation. In order to do this, it is necessary to *augment* the Hamiltonian operator: the procedure leads to additional terms which have exactly the same

[2] Since the pseudo-wavelets are not orthogonal their projectors are not simply the associated bras of the given kets.

[3] The number operator $\hat{S}$ is also known as the *overlap* operator. We here adopt the former notation in order to avoid confusion with the overlap integrals defined in (4).

role as that of the pseudopotentials in standard PW calculations. The inclusion of augmented elements will also affect therefore the procedure for MLWF calculation (see below).

Moving to the USPP framework, the generalization introduced by Vanderbilt [21] is twofold. (i) More than one projector per angular momentum channel can be taken into account: the inclusion of multiple projectors per channel enlarges the energy range [27, 21] over which logarithmic derivatives are comparable with the full potential case, thus increasing the overall portability of the pseudopotential. (ii) By relaxing the norm conservation constraint of the reference pseudo-states, the pseudo-wavefunctions are smoothed: thus, the required cut-off energy for PW representation can be drastically lowered. The fact that properties (i) and (ii) are verified for the PAW wavelets ϕ_i establishes the connection between the PAW and USPP methods. In fact, (i) is naturally valid for the wavelets $\phi_i^{\rm ps}$, because these form a basis set, and therefore have in principle an infinite number of states for each angular momentum channel; (ii) is valid as well, and the possibility of non-norm conservation in passing from $|\phi_i^{\rm ae}\rangle$ to $|\phi_i^{\rm ps}\rangle$ is accounted for by non-zero q_{ij}^I terms in (9), (10). Consequently, the PAW theory for wavefunction reconstruction can be basically adopted also in the case of USPP [28, 24].

While the PAW method is in principle an exact AE (frozen-core) approach,[4] the USPP method adopts a further approximation [24],[5] represented by the requirement of pseudizing the augmentation densities $Q_{ij}^I(\mathbf{r})$ (9). Since these terms contain the AE reference states, they are not simply writable on a PW basis: the USPP pseudization is done to make them suitable for a PW representation. This also means that the total density from (13) would be PW representable within such an approach. Even though the augmentation densities are pseudized, they must capture some features of the physical AE density. Consequently, their PW cut-off energy may be larger than the one associated with the pseudo-wavefunction density ($n^{\rm ps}(\mathbf{r})$ in (13)).

2.3. Maximally localized Wannier functions within PAW/USPP

As mentioned in section 2.1, Bloch wavefunctions enter the calculation of MLWFs only through the overlap matrix elements $M^{\mathbf{k},\mathbf{b}}$, defined in (4). Therefore, the reconstruction of these integrals from the knowledge of pseudo-wavefunctions completely solves the problem of computing MLWFs within a PAW/USPP formalism. Once overlap matrices have been calculated, we no longer distinguish between whether the parent Bloch wavefunctions were pseudized or not.

The overlaps being $M_{mn}^{\mathbf{k},\mathbf{b}}$ (4), the matrix elements of the local operator $\mathrm{e}^{-\mathrm{i}\mathbf{b}\cdot\hat{\mathbf{r}}}$, we built up the corresponding augmentation by setting $A(\hat{\mathbf{r}}) = \mathrm{e}^{-\mathrm{i}\mathbf{b}\cdot\hat{\mathbf{r}}}$ in (11). Exploiting the translational symmetry of the crystal, overlaps can be written as

$$M_{mn}^{\mathbf{k},\mathbf{b}} = \langle u_{\mathbf{k},m}^{\rm ps} | u_{\mathbf{k}+\mathbf{b},n}^{\rm ps} \rangle + \sum_{I,ij} Q_{ij}^I(\mathbf{b}) \langle \psi_{\mathbf{k},m}^{\rm ps} | \beta_{Ii}^{\mathbf{k}} \rangle \langle \beta_{Ij}^{\mathbf{k}+\mathbf{b}} | \psi_{\mathbf{k}+\mathbf{b},n}^{\rm ps} \rangle, \tag{14}$$

where we have defined

$$Q_{ij}^I(\mathbf{b}) = \int \mathrm{d}\mathbf{r}\, Q_{ij}^I(\mathbf{r}) \mathrm{e}^{-\mathrm{i}\mathbf{b}\cdot\mathbf{r}}, \tag{15}$$

$$\beta_{Ii}^{\mathbf{k}}(\mathbf{r}) = \frac{1}{\sqrt{N_k}} \sum_{\mathbf{R}} \mathrm{e}^{\mathrm{i}\mathbf{k}\cdot\mathbf{R}} \beta_{Ii}(\mathbf{r} - \mathbf{R}). \tag{16}$$

Summation over ions I in (14) is done in a single unit cell. Details of the calculation of these quantities are reported in appendix B. We stress that the scalar product of $|u^{\rm ps}\rangle$ functions cannot

[4] The PAW formalism is presented here in a all-electron frozen-core fashion but a full all-electron implementation is also compatible with the theory [22].

[5] Other differences between PAW and USPP approaches arise in the form of the effective (pseudo)potential acting of the pseudo-wavefunctions. See e.g. [22] for a more detailed discussion.

be simply augmented by the $\hat{S}$ (12) operator like those involving $|\psi^{\rm ps}\rangle$'s. In order to work with the periodic part $|u^{\rm ps}\rangle$ of the Bloch functions, *first* we have to reconstruct the AE Bloch states by means of $\hat{T}$ and *then* we can obtain the required $|u^{\rm ps}_{\mathbf{k},m}\rangle$ states by applying the local operator $\mathrm{e}^{-\mathrm{i}\mathbf{k}\cdot\hat{\mathbf{r}}}$. Since this last operator does not commute with $\hat{T}$, we are not allowed to directly work on $|u^{\rm ps}\rangle$ with the reconstruction operator. In the first scalar product of (14) the number operator $\hat{S} = \hat{T}^\dagger\hat{T}$ has been therefore substituted by the augmented operator $\hat{M} = \hat{T}^\dagger \mathrm{e}^{-\mathrm{i}\mathbf{b}\cdot\hat{\mathbf{r}}}\,\hat{T}$. We thus need to introduce the Fourier transform of the augmentation densities $Q^I_{ij}(\mathbf{b})$ instead of the augmentation charges q^I_{ij}. We also note that in the thermodynamic limit the $\mathbf{k}$-point grid becomes a continuum, so that $\mathbf{b} \to \mathbf{0}$. This limit leads to identical $\hat{S}$ and $\hat{M}$ operators. Therefore, within discrete $\mathbf{k}$-meshes the use of $\hat{S}$ instead of $\hat{M}$ is an approximation expected to give the best performance in the limit of a large number of $\mathbf{k}$-points. We will refer to this approximation as the thermodynamic limit approximation (TLA). We will comment more on its numerical aspects in section 3.

The problem of calculating Wannier functions within USPP has also been faced elsewhere [32–34]. In a first attempt, Vanderbilt and King-Smith [32] extended the calculation of the spontaneous polarization through the Berry phase [9, 10, 8] to the USPP procedure. Since the Berry phase [10] is directly related to overlap integrals, an expression for its calculation is reported in (23) of [32]. This expression adopts the $\hat{S}$ number operator instead of $\hat{M}$. Therefore, the result does not completely agree with the one presented here (14), but it can be read as an approximating formula having the right thermodynamic limit in view of the above discussion. Bernasconi and Madden [33, 34] derived instead the formalism for MLWFs with USPP in a simplified approach [35] valid only in the case of Γ-sampled supercells. Although the basic ingredients (e.g. overlaps) are the same, our treatment is valid for generic periodic systems, and recovers the Γ-only calculation as a special case. Furthermore, the proof given in [33] cannot be straightforwardly extended to the more general PAW case. The authors generalized the augmentation operator for the density (13) also to the case of the density matrix and then derived the augmentation for the $\mathrm{e}^{-\mathrm{i}\mathbf{G}_i\cdot\hat{\mathbf{r}}}$ operator. Here instead the $\mathbf{G}_i$ are the generators of the reciprocal lattice. We note that the result of Bernasconi and Madden is coherent with our treatment, while the first one of Vanderbilt and King-Smith [32] is not. Following Bernasconi and Madden, Thygesen and co-workers [36] recently derived an expression for overlap matrices within USPP for periodic systems, considering a Γ-only supercell containing the whole crystal.

Closing this section we wish to underline that matrix elements of the form $\langle\psi_{\mathbf{k},m}|\mathrm{e}^{-\mathrm{i}(\mathbf{q}+\mathbf{G})\cdot\hat{\mathbf{r}}}|\psi_{\mathbf{k}+\mathbf{q},n}\rangle$ enter also into other physical problems. A particularly appealing case is the calculation of the one-particle Green function in the GW approximation [37, 38]. Current implementations [39–41] of the method experience DFT wavefunctions mainly through the above defined matrix elements, while no direct access to the density is required. The extension of GW calculations to the case of PAW [42, 43] or USPP is therefore feasible along the same lines as we presented here for Wannier functions. We note, however, that the numerical cost is extremely higher due to the larger number of overlaps to be computed.

2.4. Numerical details

In this section we would like to describe some issues related to the numerical performance of the method. We implemented this formalism in the freely available WanT code [44], for the calculation of electronic and transport properties with WFs. We also took advantage of the complete integration of the WanT code with the PWscf package [45], which explicitly treats the DFT problem using USPPs. From here on we focus on the USPP formalism, even though a large part of the discussion is still valid also in the PAW case. The most important

advantage of using the USPP construction for Wannier functions is the scaling of the original DFT calculations, which has been described elsewhere [30]. However, this scaling also has an effect on the actual computation of WFs and we analyse this aspect in detail.

As we described above, almost the whole of the changes induced by the USPP description (relative to NCPP) in the calculation of MLWFs is related to the implementation of (14). Details on how to compute $|\beta_i^{\mathbf{k}}\rangle$ and $Q_{ij}(\mathbf{b})$ are reported in appendix B. Since no reference to the charge is made, only the very smooth wavefunction grid is used throughout the calculation. While a linear scaling with the number of plane waves is exploited in the first term (pseudo-overlaps) of (14), scalar products between projectors and pseudo-states in the second term (augmentation overlaps) are the price to pay for introducing USPPs. When we consider that the number of β projectors N_β is of the same order as the number of bands N_b (but usually larger by a factor between one and two), we see that the pseudo-state and augmentation overlap terms have the same scaling, namely $N_\mathrm{b}^2 \times N_\mathbf{k} \times N_\mathrm{PW}$. However, the pseudo-overlaps turn out to have a larger prefactor[6] and represent the leading term. Usually, USPPs allow for a reduction of the PW cut-off by a factor of 2–3 for first-row elements, up to 5 or even more for atoms with d or f states. This leads to a reduction of the PW number N_PW by a factor of around 3–10 or more. Even if the scaling w.r.t. N_PW is linear, it more than compensates the effort of augmenting overlaps and makes the introduction of USPPs numerically advantageous. Our experience shows that USPPs avoid the creation of bottlenecks in the computation of overlaps and make the WF localization the leading part of the calculation.

Finally, we note that in order to give a guess for the iterative minimizations involved in the MLWF method, it is sometimes required to compute the projections of Bloch states onto some starting localized functions [6, 7]. The augmentation of scalar products is performed as usual accounting for the $\hat{S}$ number operator (12). Projections on the β-functions are required as well, but they have already been computed and it turned out that scaling is linear w.r.t. the PW number as before. Therefore, no implications on the above discussion arise.

3. Applications

In this section we apply the above described formalism to some test cases, ranging from periodic crystals to isolated molecules. To be precise, we study fcc copper bulk, wurtzite AlN, and Watson–Crick DNA base pairs. We address a number of physical properties connected to Wannier functions: interpolation of the electronic structure, calculation of dipole moments and spontaneous polarization, analysis of the chemical bonding. All the calculations are performed with both norm-conserving and ultrasoft pseudopotentials. The numerical implications in using the USPP-TLA approach for the augmentation of overlaps are also discussed. We choose very simple systems for which MLWFs can be computed also with NCPPs and USPPs are not required. These choices allow us to test directly the USPP accuracy against the standard accuracy of the NCPP framework, for which a bibliographic record exists.

3.1. Copper bulk

We compute MLWFs for fcc copper, which has already been used as a test case in the literature [7, 34, 36] for WFs. We adopt a $6 \times 6 \times 6$ mesh of **k**-points to sample the Brillouin zone and compute six WFs corresponding to the lowest s–d manifold. In the disentanglement procedure [7] (used to get the optimal subspace for WF localization) we *freeze* the Bloch

[6] This fact comes first due to the presence of the sum over **b**-vectors (giving a prefactor from 3 to 6) and secondly because the coupling of different **k**-points for pseudo-overlaps makes wavefunction handling more cumbersome.

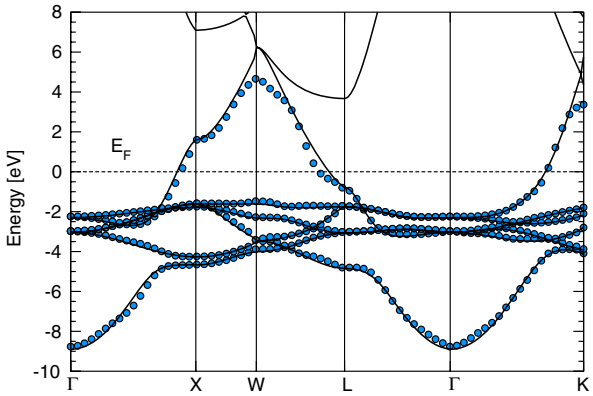

Figure 1. The fcc copper band structure: solid lines represent DFT Kohn–Sham bands (USPP) while dotted lines are results calculated using WFs.

eigenstates below the Fermi energy (*frozen states*): this means that the subspace is constructed from these selected states plus a mixture of the states above the Fermi level.

We note that no symmetry constraint is imposed *a priori* on the WF set: therefore the computed functions do not have in principle a well defined symmetry. We note that different approaches dealing with symmetry-based WFs for the current class of systems can be found in the literature [4, 5].

We adopt a kinetic energy cut-off for wavefunctions of 120 Ryd (25 Ryd) when using NCPP (USPP) and of 480 Ryd (200 Ryd) for the density. In figure 1 we superimpose the band structure directly computed from a USPP-DFT calculation and that obtained from Wannier function interpolation [6, 7, 14] on the adopted $8 \times 8 \times 8$ uniform **k**-point grid. These two sets of bands are almost superimposed below the Fermi energy and some slight differences arise only at higher energies. This is expected due to the choice of the energy window for the *frozen states*[7]: while the eigenvalues for the **k**-points in the adopted regular mesh are the same as those from the DFT calculation by construction, it is not trivial that the band structure along a generic Brillouin zone line is well reproduced. This is indeed the case here, being a signature of proper localization of the computed WFs. The band structure interpolation obtained from NCPP is essentially the same as the one in figure 1 and it is not reported. Some small discrepancies between NCPP and USPP interpolated bands are also present in the starting DFT calculations and are not of interest to us in this context.

In table 1 we report a more detailed description of quantities related to WFs (spreads, real space decay of the Hamiltonian matrix elements) in order to compare the NCPP and USPP approaches. A measure of the Hamiltonian decay is defined as

$$d(\mathbf{R}) = \left(\frac{1}{N_w} \sum_{mn} |H_{mn}(\mathbf{R})|^2 \right)^{1/2}, \tag{17}$$

where we defined $H_{mn}(\mathbf{R}) = \langle w_{\mathbf{0},m} | H | w_{\mathbf{R},n} \rangle$. These quantities are significant as a signature of the localization of the WFs used to compute the matrix elements (the more localized the WFs, the more rapidly the H matrix elements decay in space).

USPP results appear to be in very good agreement with those related to NCPP, most of the differences being reasonably due to the pseudopotential generation and not to the WF

[7] Frozen states in the disentanglement procedure are described in detail in [7].

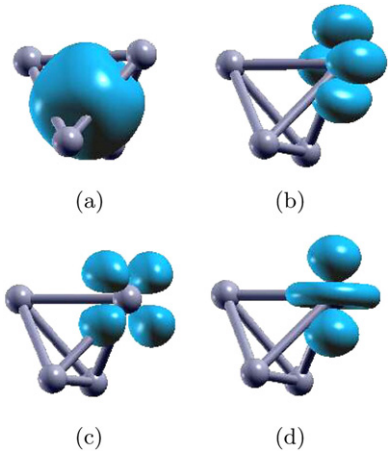

Figure 2. For fcc copper: the charge distribution for WFs computed using USPP. (a) Interstitial WF, $\Omega_a = 11.28$ Bohr^2; (b)–(d) d-character WFs, $\Omega_b = 1.86$ Bohr^2, $\Omega_c = 2.70$ Bohr^2, $\Omega_d = 1.54$ Bohr^2. The two additional d-like WFs not reported here are strictly similar to (b) and (c) by virtue of symmetry relations.

Table 1. For fcc copper: WF spreads (Bohr^2) and real space decay of the Hamiltonian matrix elements (eV) for NCPP, USPP and USPP in the thermodynamic limit approximation (USPP-TLA). Ω is the total spread, Ω_I, Ω_D and Ω_{OD} are the invariant, diagonal and off-diagonal terms, according to (A.3). $d(\mathbf{R})$ is a measure of the spatial decay of the Hamiltonian on the WF basis, as described in (17). $\boldsymbol{\tau}$ is the (0.5 0.5 0.0) direct lattice vector.

	NCPP	USPP	USPP-TLA
Ω	22.434	23.010	18.886
Ω_I	14.767	15.629	11.303
Ω_{D+OD}	7.667	7.381	7.583
$d(\boldsymbol{\tau})$	0.4876	0.4795	0.4779
$d(2\boldsymbol{\tau})$	0.0493	0.0473	0.0476
$d(3\boldsymbol{\tau})$	0.0203	0.0207	0.0205

computation. The average number of iterations required to converge the disentanglement and the localization procedures are almost the same, as are the singular spread values for the WFs. Figure 2 reports the spatial distribution of WFs from USPP calculations. As in previous works [7, 36], we find one interstitial s-like WF with the largest spread (figure 2(a)), and five more localized d-like WFs (figures 2(b)–(d)), correctly reproducing the physical s–d picture of copper.

As a last remark for the case of copper, we analyse the effect of neglecting the $e^{-i\mathbf{b}\cdot\mathbf{r}}$ term in (14), i.e. the USPP thermodynamic limit approximation (USPP-TLA). The theoretical background has already been discussed in section 2.3; here we focus on the numerical aspects. In table 1 the third column reports the results of the calculation performed within this approximation: it is evident that the numerical values of the USPP-TLA spreads deviate from the NCPP ones much more than the USPP do. In contrast, the interpolated band structure and the real space decay Hamiltonian matrix elements are definitely well suited and comparable with those obtained in the full USPP treatment. Since the TLA is known to become exact in the thermodynamic limit, we expect it to work better when increasing the dimension of the **k**-point mesh. We checked the behaviour of the approximation with respect to different meshes but no convergence could be reached for grids ranging from $4 \times 4 \times 4$ to $10 \times 10 \times 10$ **k**-points.

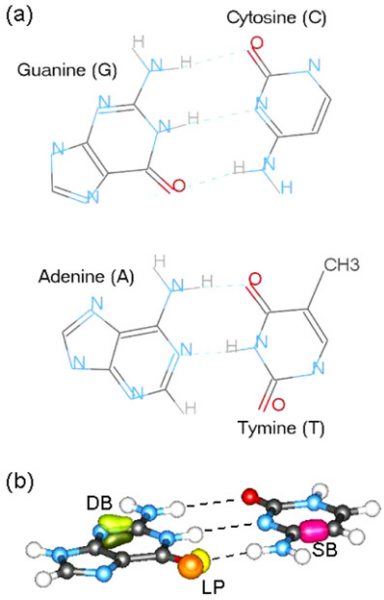

Figure 3. DNA bases. (a) Chemical schemes of the four DNA bases (G, C, A, T) assembled in the two Watson–Crick base pairs (GC and AT). (b) Isosurface plots of selected MLWFs for the GC base pair, representing a single C–C bond (SB), a double N=C bond (DB) and two oxygen lone pairs (LP). Dashed lines represent hydrogen bonds that bind the base pairs.

3.2. Isolated molecules: DNA bases and base pairs

Maximally localized Wannier functions[8] have been widely used to characterize the electrostatic properties of several molecular systems ranging from e.g. water [47–49] and small molecules [50–53] to large biomolecules, such as proteins [54], nucleic acids [55, 56], enzymes [57] and ionic channels [58]. In fact, the Wannier transformation allows one to partition the charge density into localized distributions of charges sitting on the so-called Wannier centres $\langle\hat{\mathbf{r}}\rangle_n$ [8, 9]. In the case of isolated molecular systems, the dipole moment is a well defined quantity given by $\mathbf{p} = \mathbf{p}_{\rm ion} + \mathbf{p}_{\rm el}$ with

$$\begin{aligned} \mathbf{p}_{\rm ion} &= +e\sum_{\rm I} Z_{\rm I}\mathbf{R}_{\rm I}, \\ \mathbf{p}_{\rm el} &= -2e\sum_{n}^{occ}\langle\hat{\mathbf{r}}\rangle_n, \end{aligned} \tag{18}$$

where $\mathbf{p}_{\rm ion}$ and $\mathbf{p}_{\rm el}$ are the ionic and electronic components respectively; e is the electron charge; the I summation is over the ionic sites $\mathbf{R}_{\rm I}$ and $Z_{\rm I}$ is the valence charge of the Ith atom, as defined by the corresponding pseudopotential; the n summation is over the doubly occupied valence states.

As a key test, we calculated the dipole moments of the four isolated DNA bases: guanine (G), cytosine (C), adenine (A) and thymine (T), and of the two Watson–Crick base pairs G–C and A–T, whose structures are reported in figure 3(a).

[8] For isolated systems, which can be viewed as the limiting case of periodic systems in the Γ-only sampling of the BZ, MLWFs match the well known localization criteria proposed by Boys in [46] giving raise to *Boys orbitals*. See e.g. [35, 34] for more details.

Table 2. *DNA bases*: Dipole moments |**p**| (Debye) for isolated nucleobases (G, C, A, T) and for Watson–Crick base pairs (G–C, A–T). Present work results for both USPP and NCPP approaches are compared with previous quantum chemistry HF/6-31G** calculations [59] and experimental data.

	USPP	NCPP	HF/6-31G**	Exp.
G	7.1	7.2	7.1	7.1[a]
C	6.7	6.9	7.1	7.0[b]
A	2.3	2.3	2.5	2.5[a]
T	4.2	4.4	4.6	4.1[c]
G–C	4.9	4.9	6.5	
A–T	1.7	1.8	2.0	

[a] Reference [60].
[b] Reference [61].
[c] Reference [62].

We simulated each system in a large $(22 \times 22 \times 22)$ Å^3 supercell, which allows us to avoid spurious interactions among neighbour replicas. For isolated systems, the uniform **k**-point grid reduces to the case of the Γ point only, and the connecting vectors **b** (4) correspond to the generators of the reciprocal lattice vectors. We expanded the electronic wavefunctions (charge density) up to a kinetic energy cut-off of 25 (200) and 80 (320) Ryd, using USPP and NCPP respectively.

We first optimized the atomic structure of the two base pairs G–C and A–T until the forces on all atoms were lower than 0.03 eV Å^{-1}, using ultrasoft pseudopotentials. Then, keeping atoms fixed in the relaxed geometry, we calculated the electronic structure and the corresponding MLWFs for both the single bases and the base pairs. We maintained the same geometries also for the corresponding NCPP calculations. In this case we have checked that forces on single atoms never exceeded the value of 0.05 eV Å^{-1}.

Our results for both sets of calculations are reported in table 2. We note a very good internal agreement between the USPP and NCPP cases, as well as in comparison with previous quantum chemistry HF/6-31G** calculations [59] and experimental results.

As a benchmark, we have also computed the dipole of guanine from the plane-wave charge density, obtaining a difference of 0.04 (0.08) Debye for USPP (NCPP) w.r.t. the value computed by means of WFs and reported in table 2. These small deviations measure the precision of the results based on WFs, and we checked that it can be controlled, i.e. made smaller and smaller, by increasing the simulation cell.

The total spread Ω and its components $\Omega_{\rm I}$, $\Omega_{\rm OD}$ (not shown) are also very similar in the two sets of calculations, while the diagonal term $\Omega_{\rm D}$ is, by definition [6], identically zero for isolated systems.

Finally, we can take advantage of the calculated Wannier functions to further investigate the electronic distribution and the bonding pattern in the molecules [63]. For example, as shown in figure 3(b) for the case of the G–C base pair, we are able to characterize different kinds of bonds. The SB Wannier function represents a single σ bond: it is centred in the middle point of the C–C bond. The two DB WFs describe instead a double N=C bond: this bond is partially polarized with a slight charge accumulation near the nitrogen atom. Finally, the LP WFs represents two electron lone pairs localized around the oxygen atom of the guanine molecule. Note also that the distribution of single/double bonds correctly reflects the theoretical one reported in figure 3(a). Let us remark here that our benchmark for assessing the success of the newly developed USPP-WF methodology is its relative performance with respect to the NCPP-WF (already established) framework, namely the comparison between columns 2 and 3 in table 2.

Table 3. *AlN*: electronic spontaneous polarization (C m^{-2}) of the wurtzite structure. The results presented (NCPP, USPP and USPP-TLA) are compared to the literature. As a reference we also report the invariant (Ω_I) and the total spread (Ω; Bohr^2) given by the WF calculations for wurtzite. Results from [12] are obtained using GGA and LDA (in parentheses) respectively.

P_{SP}	NCPP	USPP	USPP-TLA
This work	−0.081	−0.080	−0.080
Ref. [12]			−0.090 (−0.099)
Ref. [68]		−0.120	
Ω	80.895	80.756	80.271
Ω_I	67.683	67.857	67.282

3.3. AlN wurtzite

Here we move to the calculation of polarization in periodic systems. See the review by Resta [8] for a more detailed description. We focus on the case of aluminium nitride and compute the spontaneous polarization P_{SP} of the wurtzite phase. This is a particularly appealing test case since a large debate exists in the literature and many results are present [64–68, 12, 69]. Moreover, nitrogen may be more easily described (in terms of PW kinetic energy cut-off) with USPPs than with NCPPs, allowing for an advantageous application of the current formalism. Following [12, 70] we evaluate the polarization (electronic and ionic contributions) for the wurtzite (WZ) phase taking the zinc-blende (ZB) structure as a reference. Our calculations adopt the GGA-PBE parametrization for the exchange–correlation functional, and use cut-off energies of 60 Ryd (25 Ryd) for NCPP (USPP) for wavefunctions and 240 Ryd (200 Ryd) for the density.

We relax both the cell dimensions and the atomic positions of the WZ phase. The ZB reference is assumed to have ideal atomic positions and the cell is taken to have the same volume (but not the shape) as the one computed for the WZ polytype (six bilayers are included in the cell). These structural calculations have been performed using USPP and the (lattice and ionic) parameters obtained have been used also in the NCPP simulations. Using a $16 \times 16 \times 4$ Monkhorst–Pack [71] mesh of **k**-points we obtained the a and c/a parameters of the hexagonal lattice as $a = 3.1144$ Å and $c/a = 1.6109$ (for the standard WZ cell including two bilayers; $c/a = 4.8326$ for the actual cell we adopted). The resulting ZB cell has the ideal parameter $c/a = 4.899$ while $a = 3.1002$ Å.

In table 3 we report the comparison of USPP and NCPP results in our calculations as well as other results from the literature. We estimate the numerical accuracy of the calculation to be of the order of 0.005 C m^{-2}. The values of spontaneous polarization computed using NCPPs are almost identical to those obtained with USPPs ($P_{SP} = -0.080$ C m^{-2}). The USPP-TLA behaves very accurately in this case and no difference can be found with respect to the full USPP calculation. Our results are also in nice agreement with the USPP-TLA calculation by Bernardini *et al* [12], who used a Berry-phase formalism [9] and found a value of $P_{SP} = -0.090$ C m^{-2}. We thus conclude that the USPP-TLA approximation performs well for the computation of the spontaneous polarization in nitrides, relative to a pure USPP treatment without the thermodynamic limit approximation.

These results for the P_{SP} in AlN wurtzite are also in agreement with indirect experimental evidence as reported in [67, 66, 69]. While some earlier experimental fits [72, 73] claim much lower values of P_{SP} (ranging from −0.040 to −0.060 C m^{-2}), later [69, 74] works explain this discrepancy as due the neglecting of bowing effects (non-linearity) of the P_{SP} with respect to the composition of the alloy $Al_xGa_{1-x}N$ employed in the measurements.

4. Conclusions

In this paper we presented an approach for calculating *maximally localized Wannier functions* in the general framework of the PAW theory. This formalism then recovers the USPP framework as a special case. The main advantage of using PAW/USPP over NCPP is the well known reduction of the computational effort in the evaluation of the electronic wavefunctions at the DFT level. This leads to a consequent reduction of computational load also in the calculation of MLWFs. Furthermore, the reformulation within the PAW scheme allows us to interface the computation of MLWFs to other popular approaches for the electronic structure calculation. Finally, our method is formulated in the case of a uniform **k**-point mesh for the sampling of the Brillouin zone (BZ), which includes (but is more general than) a previous attempt based on Γ-only calculations. This allows us to treat periodic solid-state systems (such as crystals, surfaces and interfaces), which require a full description of the BZ, as well as molecular, finite or amorphous systems which are well described with the Γ-only representation.

As a first illustration of the capability of this methodology, we presented the calculation of the MLWFs for a few selected test cases, easily referable to well established theoretical and experimental results. For each selected system we also compared the results for both USPP and NCPP calculations, underlining a very good agreement between the two cases.

The reduction of the computational cost resulting from USPP calculations opens the way to the exploitation of the MLWFS as a powerful tool for analysing the electronic structure of larger and more realistic nanoscale systems, in particular for transport in nanojunctions [14, 15].

Acknowledgments

We acknowledge discussions on the USPP formalism with Giovanni Bussi, Marco Buongiorno Nardelli and Elisa Molinari for the treatment of USPP. Funding was provided by the EC through TMR network 'Exciting', by INFM through 'Commissione Calcolo Parallelo', by the Italian MIUR through PRIN 2004, and by the regional laboratory of EM 'Nanofaber'. Parts of the figures were realized using the XCrySDen package [75].

Appendix A. Main formulae for maximally localized Wannier functions

For the sake of completeness we report here the main relations [6] entering the expression (3) for the spread functional $\Omega[U]$ and its first derivative w.r.t. the unitary transformation U. These are all the quantities involved in the minimization procedure for the calculation of maximally localized Wannier functions. The expectation values of the position operator are

$$\langle \mathbf{r} \rangle_n = -\frac{1}{N} \sum_{\mathbf{k},\mathbf{b}} w_{\mathrm{b}} \mathbf{b} \operatorname{Im} \ln M_{nn}^{\mathbf{k},\mathbf{b}}, \tag{A.1}$$

$$\langle r^2 \rangle_n = \frac{1}{N} \sum_{\mathbf{k},\mathbf{b}} w_{\mathrm{b}} \left\{ \left[1 - |M_{nn}^{\mathbf{k},\mathbf{b}}|^2 \right] + \left[\operatorname{Im} \ln M_{nn}^{\mathbf{k},\mathbf{b}} \right]^2 \right\}, \tag{A.2}$$

where **b**-vectors connect nearest-neighbour **k**-points and w_{b} are their weights according to appendix B of [6].

To make the Ω dependence on the overlap explicit, the spread functional can be divided into three terms, the invariant (I), the diagonal (D) and the off-diagonal (OD) components [6]:

$$\Omega[U] = \Omega_{\mathrm{I}} + \Omega_{\mathrm{D}}[U] + \Omega_{\mathrm{OD}}[U], \tag{A.3}$$

whose definitions are, respectively,

$$\Omega_{\rm I} = \frac{1}{N}\sum_{\mathbf{k},\mathbf{b}} w_{\rm b}\left(N_w - \sum_{mn}|M_{nn}^{\mathbf{k},\mathbf{b}}|^2\right), \tag{A.4}$$

$$\Omega_{\rm D} = \frac{1}{N}\sum_{\mathbf{k},\mathbf{b}} w_{\rm b}\sum_{n}\left({\rm Im}\ln M_{nn}^{\mathbf{k},\mathbf{b}} + \mathbf{b}\cdot\mathbf{r}_n\right)^2, \tag{A.5}$$

$$\Omega_{\rm OD} = \frac{1}{N}\sum_{\mathbf{k},\mathbf{b}} w_{\rm b}\sum_{m\neq n}|M_{mn}^{\mathbf{k},\mathbf{b}}|^2. \tag{A.6}$$

Appendix B. Detailed expressions for the calculation of $|\beta_i^{\mathbf{k}}\rangle$ and $Q_{ij}(\mathbf{b})$

We report the explicit expression for the calculation of the reciprocal space representation of the PAW/USPP projectors and the Fourier transform of the augmentation densities:

$$Q_{ij}^I(\mathbf{b}) = \int {\rm d}\mathbf{r} {\rm e}^{-{\rm i}\mathbf{b}\cdot\mathbf{r}} Q_{ij}^I(\mathbf{r}-\boldsymbol{\tau}_{\rm I}). \tag{B.1}$$

Here we made explicit the dependence of $Q_{ij}^I(\mathbf{b})$ on the atomic position $\boldsymbol{\tau}_{\rm I}$. These tasks are also required in the evaluation of e.g. the density in reciprocal space and are therefore performed in standard plane-wave DFT codes.

The indices i, j in $\beta_i(\mathbf{r})$ and $Q_{ij}(\mathbf{r})$ stand for radial and angular numbers, e.g. $n_i l_i m_i$. Projectors and augmentation densities are explicitly written as products of a radial part and (real) spherical harmonics:

$$\beta_i(\mathbf{r}) = R_{n_i}(r) Y_{l_i}^{m_i}(\hat{r}) \tag{B.2}$$

$$Q_{ij}(\mathbf{r}) = g_{n_i n_j}(r) Y_{l_i}^{m_i}(\hat{r}) Y_{l_j}^{m_j}(\hat{r}). \tag{B.3}$$

First we focus on the expression for β projectors. Functions of the form $f(\mathbf{r}) = R(r)\, Y_L^M(\hat{r})$ have a known semi-analytical Fourier transform which is given by

$$f(\mathbf{k}) = 4\pi(-{\rm i})^l Y_l^m(\hat{k}) \int_0^\infty r^2 R(r) J_l(kr)\, {\rm d}r \tag{B.4}$$

where $J_l(x)$ is the spherical Bessel function of order l. The problem for β projectors is therefore directly solved once we add the structure factors accounting for the actual positions of the ion:

$$\beta_{Ii}^{\mathbf{k}}(\mathbf{G}) = 4\pi(-{\rm i})^{l_i} {\rm e}^{-{\rm i}(\mathbf{k}+\mathbf{G})\boldsymbol{\tau}_{\rm I}} Y_{l_i}^{m_i}(\hat{G}) \int_0^\infty r^2 R_{n_i}(r) J_{l_i}(Gr)\, {\rm d}r. \tag{B.5}$$

Moving to the case of the augmentation densities, we note that the product of two spherical harmonics can be expressed as a linear combination of single spherical harmonics using Clebsch–Gordan coefficients:

$$Y_{l_i}^{m_i}(\hat{r}) Y_{l_j}^{m_j}(\hat{r}) = \sum_{L=|l_i-l_j|}^{l_i+l_j} \sum_{M=-L}^{L} C_{l_i l_j m_i m_j}^{LM} Y_L^M(\hat{r}). \tag{B.6}$$

This allows us to follow the same strategy as before also for (B.3). Putting (B.4)–(B.6) together, the final expression for $Q_{ij}^I(\mathbf{b})$ reads

$$Q_{ij}^I(\mathbf{b}) = 4\pi {\rm e}^{-{\rm i}\mathbf{b}\cdot\boldsymbol{\tau}} \sum_L \sum_M C_{l_i l_j m_i m_j}^{LM} (-{\rm i})^L Y_L^M(\hat{b}) \int_0^\infty r^2 g_{n_i n_j}(r) J_L(br)\, {\rm d}r \tag{B.7}$$

where the M, L indices run as in (B.6).

References

[1] Wannier G H 1937 *Phys. Rev.* **52** 191–7
[2] Kohn W 1959 *Phys. Rev.* **115** 809–21
[3] Teichler H 1971 *Phys. Status Solidi* a **43** 307–18
[4] Sporkmann B and Bross H 1994 *Phys. Rev.* B **49** 10869–76
[5] Sporkmann B and Bross H 1997 *J. Phys.: Condens. Matter* **9** 5593–608
[6] Marzari N and Vanderbilt D 1997 *Phys. Rev.* B **56** 12847–65
[7] Souza I, Marzari N and Vanderbilt D 2001 *Phys. Rev.* B **65** 035109
[8] Resta R 1994 *Rev. Mod. Phys.* **66** 899–915
[9] King-Smith R D and Vanderbilt D 1993 *Phys. Rev.* B **47** R1651–4
[10] Vanderbilt D and King-Smith R D 1993 *Phys. Rev.* B **48** 4442–55
[11] Souza I, Martin R M, Marzari N, Zhao X and Vanderbilt D 2000 *Phys. Rev.* B **62** 15505–20
[12] Bernardini F, Fiorentini V and Vanderbilt D 2001 *Phys. Rev.* B **63** 193201
[13] Nakhmanson S M, Calzolari A, Meunier V, Bernholc J and Buongiorno Nardelli M 2003 *Phys. Rev.* B **67** 235406
[14] Calzolari A, Marzari N, Souza I and and Buongiorno Nardelli M 2004 *Phys. Rev.* B **69** 035108
[15] Ferretti A, Calzolari A, Di Felice R, Manghi F, Caldas M J, Buongiorno Nardelli M and Molinari E 2005 *Phys. Rev. Lett.* **94** 116802
[16] Ferretti A, Calzolari A, Di Felice R and Manghi F 2005 *Phys. Rev.* B **72** 125114
[17] Lee Y S, Buongiorno Nardelli M and Marzari N 2005 *Phys. Rev. Lett.* **95** 076804
[18] Thygesen K S and Jacobsen K W 2005 *Phys. Rev. Lett.* **94** 036807
[19] Hamann D R, Schlüter M and Chiang C 1979 *Phys. Rev. Lett.* **43** 1494–7
[20] Bachelet G B, Hamann D R and Schluter M 1982 *Phys. Rev.* B **26** 4199–228
[21] Vanderbilt D 1990 *Phys. Rev.* B **41** R7892–5
[22] Blöchl P E 1994 *Phys. Rev.* B **50** 17953–79
[23] Hetényi B, De Angelis F, Giannozzi P and Car R 2001 *J. Chem. Phys.* **115** 5791–5
[24] Kresse G and Joubert D 1999 *Phys. Rev.* B **59** 1758–75
[25] He L and Vanderbilt D 2001 *Phys. Rev. Lett.* **86** 5341–4
[26] Blount E I 1962 *Solid State Physics* vol 13, ed F Seitz and D Turnbull (New York: Academic) p 305
[27] Blöchl P E 1990 *Phys. Rev.* B **41** R5414–6
[28] Van de Walle C G and Blöchl P E 1993 *Phys. Rev.* B **47** 4244–55
[29] Laasonen K, Car R, Lee C and Vanderbilt D 1991 *Phys. Rev.* B **43** R6796–9
[30] Laasonen K, Pasquarello A, Car R, Lee C and Vanderbilt D 1993 *Phys. Rev.* B **47** 10142–51
[31] Giannozzi P, Angelis F D and Car R 2004 *J. Chem. Phys.* **120** 5903–15
[32] Vanderbilt D and King-Smith R D 1998 *Preprint* cond-mat/9801177v1
[33] Bernasconi L and Madden P A 2001 *J. Mol. Struct.* **544** 49–60
[34] Marzari N, Souza I and Vanderbilt D 2003 *Psi-K Newslett.* **57** 129–68
[35] Silvestrelli P L, Marzari N, Vanderbilt D and Parrinello M 1998 *Solid State Commun.* **107** 7–11
[36] Thygesen K S, Hansen L B and Jacobsen K W 2005 *Phys. Rev.* B **72** 125119
[37] Hedin L 1965 *Phys. Rev.* **139** A796–823
[38] Onida G, Reining L and Rubio A 2002 *Rev. Mod. Phys.* **74** 601–59
[39] Baroni S and Resta R 1986 *Phys. Rev.* B **33** 7017–21
[40] Hybertsen M S and Louie S G 1986 *Phys. Rev.* B **34** 2920–2
[41] Godby R W, Schlüter M and Sham L J 1988 *Phys. Rev.* B **37** 10159–75
[42] Arnaud B and Alouani M 2000 *Phys. Rev.* B **62** 4464–76
[43] Lebègue S, Arnaud B, Alouani M and Bloechl P E 2003 *Phys. Rev.* B **67** 155208
[44] Calzolari A, Ferretti A, Cavazzoni C, Marzari N and Buongiorno Nardelli M 2005 WanT code http://www.wannier-transport.org
[45] Baroni S, Dal Corso A, de Gironcoli S and Giannozzi P 2001 http://www.pwscf.org
[46] Boys S F 1960 *Rev. Mod. Phys.* **32** 296–99
[47] Berghold G, Mundy C J, Romero A H, Hutter J and Parrinello M 2000 *Phys. Rev.* B **61** 10040–8
[48] Leung K and Rempe S 2004 *J. Am. Chem. Soc.* **126** 344–51
[49] Dellago C and Naorb M M 2005 *Comput. Phys. Commun.* **169** 36–9
[50] Alber F, Folkers G and Carloni P 1999 *J. Phys. Chem.* B **103** 6121–6
[51] Mantz Y, Gerard H, Iftimie R and Martyna G 2004 *J. Am. Chem. Soc.* **126** 4080–1
[52] Kuo I F and Tobias D 2001 *J. Phys. Chem.* B **105** 5827–32
[53] Gaigeot M and Sprik M 2003 *J. Phys. Chem.* B **107** 10344–58
[54] Sulpizi M and Carloni P 2000 *J. Phys. Chem.* B **104** 10087–91
[55] Mundy C, Colvin M and Quong A 2002 *J. Phys. Chem.* A **106** 10063–71

[56] Magistrato A, Ruggerone P, Spiegel K, Carloni P and Reedijk J 2006 *J. Phys. Chem.* B **110** 3604–13
[57] Cavalli A and Carloni P 2002 *J. Am. Chem. Soc.* **124** 3763–8
[58] Guidoni L and Carloni P 2002 *Biochim. Biophys. Acta* **1563** 1–6
[59] Sponer J and Hobza J L P 1996 *J. Phys. Chem.* **100** 1965–74
[60] DeVoe H and Tinoco I Jr 1962 *J. Mol. Biol.* **4** 518–27
[61] Weber H and Craven B 1990 *Acta Crystallogr.* B **46** 532–8
[62] Kulakowski I, Geller M, Lesyng B and Wierzcho K 1974 *Biochim. Biophys. Acta* **361** 119–30
[63] Foster J and Boys S 1960 *Rev. Mod. Phys.* **32** 300–2
[64] Bernardini F and Fiorentini V 1998 *Phys. Rev.* B **58** 15292–5
[65] Guy I L, Muensit S and Goldys E M 1999 *Appl. Phys. Lett.* **75** 4133–5
[66] Rizzi A, Lantier R, Monti F, Luth H, Sala F D, Carlo A D and Lugli P 1999 *J. Vac. Sci. Technol.* B **17** 1674–81
[67] Ambacher O, Smart J, Shealy J R, Weimann N G, Chu K, Murphy M, Schaff W J, Eastman L F, Dimitrov R, Wittmer L, Stutzmann M, Rieger W and Hilsenbeck J 1999 *J. Appl. Phys.* **85** 3222–33
[68] Bechstedt F, Grossner U and Furthmüller J 2000 *Phys. Rev.* B **62** 8003–11
[69] Ambacher O, Majewski J, Miskys C, Link A, Hermann M, Eickhoff M, Bernardini F M S, Fiorentini V, Tilak V, Schaff B and Eastman L F 2002 *J. Phys.: Condens. Matter* **14** 3399–34
[70] Posternak M, Baldereschi A, Catellani A and Resta R 1990 *Phys. Rev. Lett.* **64** 1777–80
[71] Monkhorst H J and Pack J D 1976 *Phys. Rev.* B **13** 5188–92
[72] Park S H and Chuang S L 2000 *Appl. Phys. Lett.* **76** 1981–3
[73] Park S H, Ahn D and Lee Y T 2001 *Japan. J. Appl. Phys.* **40** L941–4
[74] Vaschenko G, Patel D, Menoni C S, Ng H M and Cho A Y 2002 *Appl. Phys. Lett.* **80** 4211–3
[75] Kokali A 2003 *Comput. Mater. Sci.* **28** 155–68